CARBON 47 (2009) 2571–2578

available at www.sciencedirect.com

ScienceDirect

journal homepage: www.elsevier.com/locate/carbon

The effect of carbon nanotube aspect ratio and loading on the elastic modulus of electrospun poly(vinyl alcohol)-carbon nanotube hybrid fibers

Kenneth Kar Ho Wong[a], *Martin Zinke-Allmang*[a,b], *Jeffery L. Hutter*[b], *Sabahudin Hrapovic*[d], *John H.T. Luong*[d], *Wankei Wan*[c,*]

[a]*Department of Medical Biophysics, The University of Western Ontario, London, Ontario, Canada N6A 5C1*
[b]*Department of Physics and Astronomy, The University of Western Ontario, London, Ontario, Canada N6A 3K7*
[c]*Department of Chemical and Biochemical Engineering, The University of Western Ontario, London, Ontario, Canada N6A 5B9*
[d]*Biotechnology Research Institute, National Research Council Canada, Montreal, Quebec, Canada H4P 2R2*

ARTICLE INFO

Article history:
Received 20 January 2009
Accepted 7 May 2009
Available online 18 May 2009

ABSTRACT

The reinforcement effect of carbon nanotubes (CNTs) has been examined as a function of their loading and aspect ratio in poly(vinyl alcohol) (PVA) based hybird fibers. Lignosulfonic acid sodium salt (LSA) was used to disperse CNTs to produce consistently high CNT loaded PVA-LSA-CNT hybrid fibers using an electrospinning process. The elastic modulus of individual fibers was measured using atomic force microscopy. The presence of CNTs significantly increased the average elastic modulus of PVA-LSA-CNT fibers compared to PVA-LSA fibers. The elastic modulus, however, exhibited no fiber diameter dependency. Transmission electron microscopy (TEM) was used to determine the loading and the aspect ratio of CNTs in each hybrid fiber. The CNT loading in PVA-LSA-CNT fibers varied widely due to non-uniform CNT dispersion and displayed no relationship with the elastic modulus. Our results also demonstrated that the average value of CNT aspect ratio significantly affected the elastic modulus of the hybrid fibers. Such a result was in agreement with theoretical prediction in which the stress transfer efficiency in a composite matrix is strongly dependent on the CNT aspect ratio.

© 2009 Elsevier Ltd. All rights reserved.

1. Introduction

Carbon nanotubes (CNTs), first observed in 1952 [1,2], display exceptional mechanical [3], thermal [4] and electrical [5] properties. Such features have motivated the use of CNTs as nanofillers in polymer matrices to form composite materials for various applications such as filters [6], field-emission displays [7], nanosensors [8], thermal interface materials [9] and for drug delivery [10]. In 1994, Ajayan et al. [11] were the first to propose the fabrication of CNT-polymer composite materials, capitalizing on the superior mechanical properties [12] of CNTs for mechanical reinforcement [13]. The mechanical properties of CNT-polymer composite materials primarily depend on the dispersion [14], orientation [15], loading [16] and aspect ratio [17] of CNTs in the composite matrix.

For the fabrication of CNT-polymer composite materials, most methods begin with dispersing CNTs in a polymer solution. Increasing CNT concentration in the solution will decrease the uniformity of CNT dispersion, i.e. increasing CNT agglomeration (bundling) [14]. This observation thus provides

* *Corresponding author:* Fax: +1 519 850 2308.
E-mail address: wkwan@eng.uwo.ca (W. Wan).
0008-6223/$ - see front matter © 2009 Elsevier Ltd. All rights reserved.
doi:10.1016/j.carbon.2009.05.006

LGES 1022

a plausible explanation for the demonstrated improvement in mechanical properties at low concentrations but adverse effects at high concentrations [18–20]. Any less-than-ideal dispersion of CNTs can cause problems in fabricating composite materials, especially for fibers with sizes comparable to CNTs. CNT concentration in the solution (nominal loading) is not directly correlated to the physical loading in the fiber. Therefore, CNT loading can be non-uniform across the fiber and causes variability in the reinforcement effect from sample to sample.

CNT aspect ratio is one important parameter that significantly affects the amount of stress transfer from the matrix to CNTs in composite materials as shown in theoretical studies [21]. Tucker and Liang [17] summarized five different physical models, including Halpin-Tsai [22], and suggested that under strictly idealizing assumptions such as axisymmetric orientation and mono-dispersity in shape and size, the overall mechanical properties of composite materials significantly vary with the aspect ratio of the reinforced CNTs. However, these assumptions are difficult to experimentally achieve because CNTs coil and agglomerate to form bundles. Sonication is commonly used to improve CNT dispersion and prevent agglomeration, but this process often breaks the CNTs into shorter fragments at the locations of intrinsic defects [23,24]. Hence, few CNTs with sufficient lengths are retained in the matrix at nanometer scale. To date, only few consistent results from CNT reinforcement are available for composite materials. To further our understanding of CNT-polymer hybrid materials, an accurate determination of the distribution of the CNT aspect ratio is as important as determining the CNT loading inside the matrix as both factors are required to correctly predict the CNT reinforcement in composite materials.

CNT orientation is another parameter with a strong effect on properties of the composite materials [25]. Wang et al. [15] showed that the mechanical properties are improved when CNTs are aligned parallel to the applied stress. Unlike silica nanospheres or clay nanodisks, CNTs have a high aspect ratio, i.e. their orientation can change from isotropic (highly random orientation) to anisotropic (with a high fraction of aligned CNTs) and altering the properties of the composite materials. Haggenmueller et al. [26] showed that smaller spatial confinement increases the degree of CNT alignment. To achieve a high level of CNT alignment, Geo et al. [27] proposed the use of electrospinning to manufacture CNT-polymer composite nanofibers.

This paper advocates the use of lignosulfonic acid sodium salt (LSA) to effectively disperse [28] pristine CNTs in water towards the fabrication of hybrid fibers based on poly(vinyl alcohol) (PVA). PVA has good thermal stability, chemical resistance and biocompatibility [29]. Dissolved in water and ethanol, it can be used in electrospinning [30]. The elastic modulus of individual fibers is measured using atomic force microscopy (AFM) multi-points bending test [31]. Transmission electron microscopy (TEM) is used to measure the loading and the aspect ratio of CNTs in each individual hybrid fiber. Such collective results allow us to comment on the effect of fiber diameter, CNT loading and CNT aspect ratio on the mechanical properties of the hybrid fibers.

2. Experimental

2.1. Materials and processing parameters for electrospinning

7.2 wt.% PVA (M_w = 89,000–98,000 g/mol, 99+% hydrolyzed, Sigma–Aldrich), 0.8 wt.% LSA (average M_n = 3000 and M_w = 8000, Sigma–Aldrich) and 0.4 wt.% MWCNTs (hollow structure multiwalled carbon nanotubers with purity >95%, CheapTubes Inc.) were dissolved/dispersed in a solvent consisting of 75% deionized water and 25% ethanol. The solution was sonicated for 1 h prior to electrospinning. PVA-LSA-CNT hybrid fibers were electrospun using an electric field of 18 kV over a distance of 24 cm between the syringe needle and the grounded collector. The solution was fed at 0.12 ml/h. A TEM grid (with $7.5 \times 7.5\ \mu m^2$ square meshes, Structure Probe Inc.) was used on a silicon substrate to collect individual, isolated electrospun fibers at the collector.

Two additional solutions were prepared for electrospinning and produced fibers using the same procedure: (1) 7.2 wt.% PVA and 0.8 wt.% LSA in 75% deionized water and 25% ethanol and (2) 8 wt.% PVA in 80% deionized water and 20% ethanol. PVA-LSA fibers and PVA fibers were prepared and measured for comparison.

2.2. Raman spectroscopy

Raman spectra of pristine CNTs and PVA-LSA-CNT hybrid fibers were acquired by a Raman analyzer (LabRAM HR 800, Horiba/Jobin Yvon, Longjumeau, France) equipped with a frequency-doubled argon ion 514.5 nm laser operating at 100 mW (lexel 95-SHG, Cambridge Lasers Laboratories, Fremont, CA). A CCD detector at −75 °C recorded spectra with a resolution of 0.3 cm^{-1} $pixel^{-1}$ based on an 800 mm focal length of the LabRAM HR. The instrument was wavelength-calibrated with a silicon wafer based on a static spectrum centered at 521 cm^{-1}.

A scanning electron microscopy (SEM) micrograph of PVA-LSA-CNT hybrid fibers is shown in Fig. 1a. The mat consisting of the hybrid fibers was characterized using Raman spectroscopy at two different spots with the results shown as the upper two spectra in Fig. 1b. A Raman signature of CNTs (from CNT-dimethylformamide solution) was also obtained and shown in Fig. 1b. The three major Raman peaks of pristine CNTs matched in the spectra of the hybrid fibers confirmed the presence of CNTs in the polymer matrix.

2.3. AFM nanomechanical measurement

Mechanical testing of individual fibers was performed using a multi-mode AFM with a Nanoscope IIIa controller (Veeco Instruments) at room temperature and relative humidity of ⩽9% (nitrogen gas ambient). A triangular silicon nitride cantilever (NP Series Probes, Veeco Instruments) with a nominal spring constant of 0.32 N/m was chosen for imaging and mechanical testing of PVA-LSA-CNT, PVA-LSA and PVA fibers. The actual spring constant (k) was determined using the thermal noise technique [32] as $k = 0.22 \pm 0.01$ N/m. This value was periodically verified during the experiments.

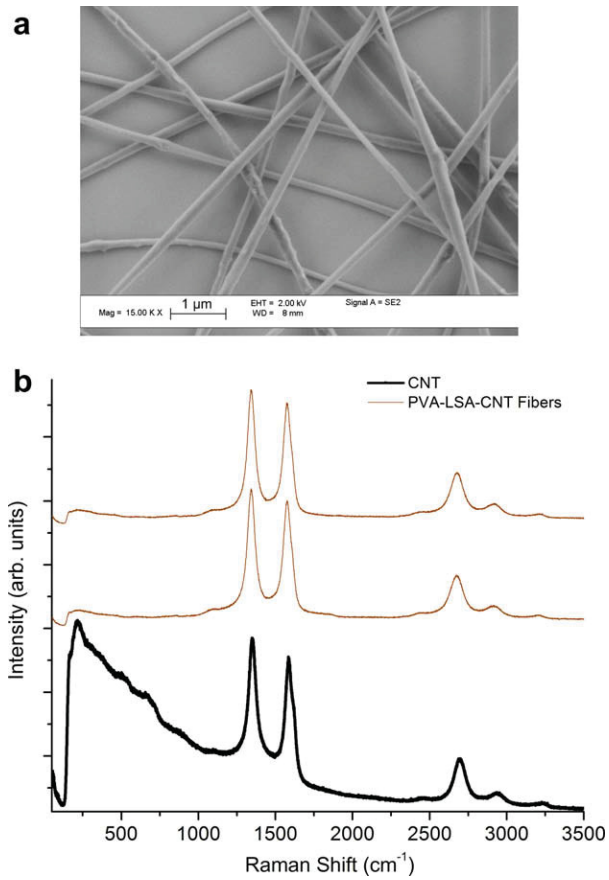

Fig. 1 – (a) SEM image of PVA-LSA-CNT fibers, (b) Raman spectra of CNT and two different spots of PVA-LSA-CNT fiber mat.

Mechanical testing was performed in the AFM force-volume mode [31]. The force spectra were acquired for positions in an array of 64×64 pixels spanning square regions of 4.0–6.5 μm width. The acquired data were extracted from the force-volume images and analyzed using the Igor Pro software package (Wavemetrics) with a custom analysis routine. The clamped beam model was used for determining the Young's modulus of the fiber [31]. 26 PVA-LSA-CNT, 22 PVA-LSA and 25 PVA fibers with suspended lengths between 3.5 and 6.5 μm were chosen on three separated TEM grids for AFM nanomechanical testing.

In each case, suitable fibers were precisely located on a TEM grid using optical microscope images prior to SEM, AFM and TEM measurements. A particular PVA-LSA-CNT fiber is shown in the SEM image of Fig. 2a (captured by Leo 1530 at 2 kV), AFM force-volume image of Fig. 2b and TEM image of Fig. 2c (captured by Hitachi S-570 at 100 kV). The fiber diameter D was determined from the SEM micrograph on the suspended portion by averaging the diameter measurements at 10 locations.

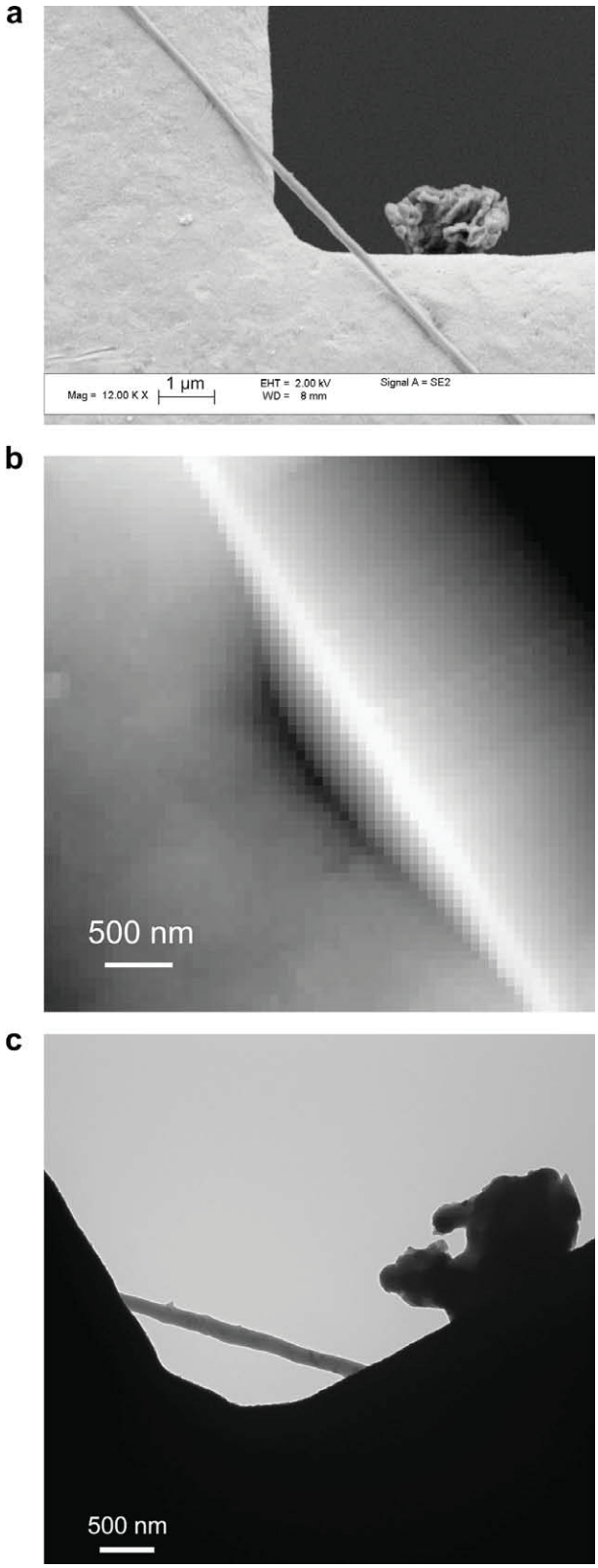

Fig. 2 – (a) SEM image, (b) AFM force-volume image, and (c) TEM image of the same PVA-LSA-CNT fiber suspended on a TEM grid.

3. Results and discussion

3.1. *Effect of the fiber diameter on the elastic modulus*

Fig. 3a shows the elastic moduli of PVA-LSA-CNT hybrid fibers with diameters ranging from 145 to 250 nm. To compare the effect of CNT reinforcement introduced into the fiber matrix, the elastic modulus of PVA-LSA (with no CNT) fibers

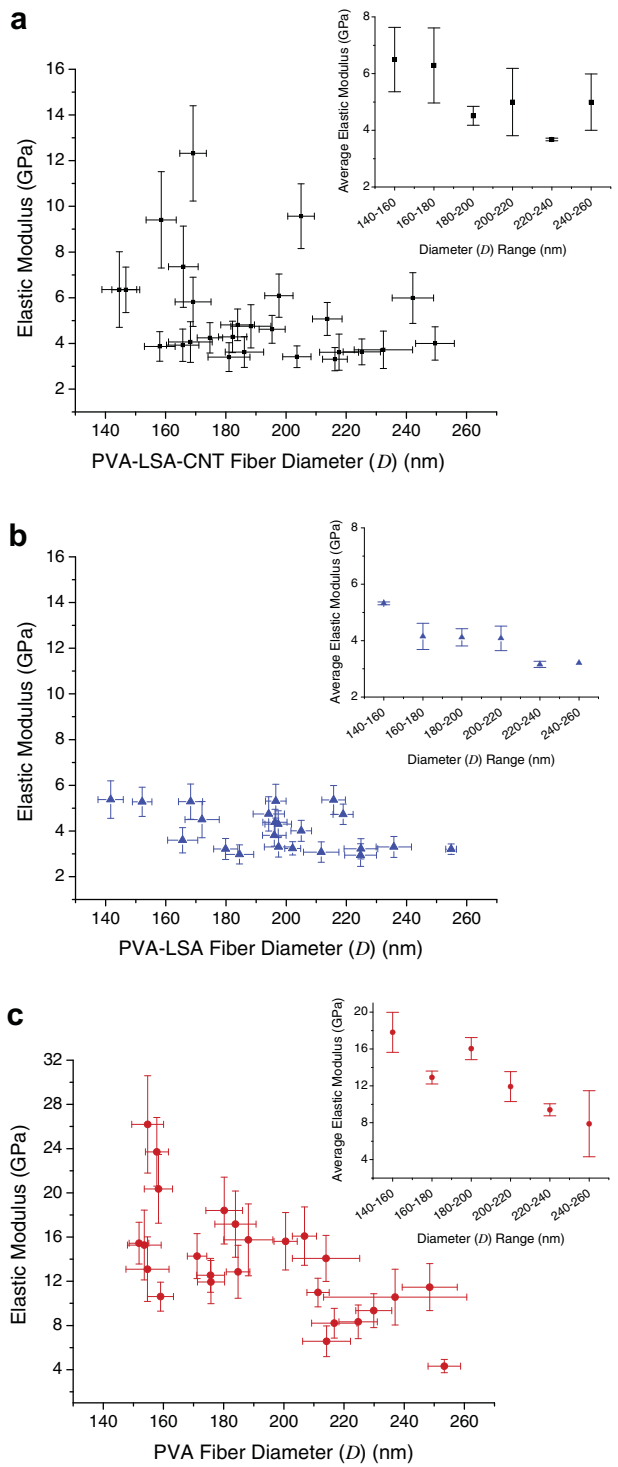

Fig. 3 – Plots of elastic modulus vs. diameter of: (a) 26 PVA-LSA-CNT, (b) 22 PVA-LSA and (c) 25 PVA fibers, with the inserts showing a profile of the average elastic modulus in each diameter range.

with a similar diameter range of 142–255 nm (Fig. 3b) and PVA fibers with 152–253 nm in diameter (Fig. 3c) were also measured. The error bars are due to the experimental uncertainties of the spring constant calibration, the measurement of the fiber diameter and the fitted parameter of the elastic modulus.

The average elastic modulus of all PVA-LSA-CNT fibers with an average diameter of 190 ± 6 nm was estimated to be 5.3 ± 0.4 GPa. The uncertainties were the standard error (SE). PVA-LSA fibers had an average elastic modulus of 4.0 ± 0.2 GPa with an average diameter of 197 ± 6 nm. PVA fibers with an average diameter of 192 ± 6 nm had an average elastic modulus of 14 ± 1 GPa. The results thus indicated that for essentially the same diameter range, there was a significant difference in elastic moduli (one-way ANOVA; $P = 0.02$) between PVA-LSA-CNT fibers and PVA-LSA fibers. PVA fibers exhibited significantly higher mean elastic modulus (one-way ANOVA; $P < 0.01$) than PVA-LSA-CNT or PVA-LSA fibers.

Each data set was divided into 6 groups based on the diameter of the fibers and plotted against the average elastic modulus (±SE) of each group as shown in the inserts of Fig. 3a–c. For the PVA-LSA-CNT hybrid fibers, one-way ANOVA results revealed that the elastic modulus had no diameter dependence as each group was insignificantly different from the others. For PVA-LSA fibers, the 140–160 nm diameter group was significantly different ($P < 0.01$) to the 220–240 nm diameter group. A comparison between the 140–160 nm and 240–260 nm could not be made as only one fiber was accounted for the latter group. All other groups with sufficient fibers were insignificantly different from each other. For PVA fibers, the 140–160 nm diameter group was significantly different ($P < 0.02$) from the three groups with diameters ranging from 200 to 260 nm. The 180–200 nm diameter group was significantly different ($P < 0.05$) to two groups between 220 and 260 nm. The remaining groups were determined to vary insignificantly.

3.2. *Effect of LSA in PVA-LSA-CNT fibers*

In order to disperse CNTs in PVA solution for electrospinning hybrid fibers, the LSA content was intentionally increased from what Liu et al. [28] proposed (1.5 mg LSA per 1 mg CNTs) to 2 mg LSA per 1 mg CNTs in the solution to induce a significant plasticizing effect [33,34]. The elastic moduli of PVA fibers exhibited a significant size-dependence, increasing from 8 to 17 GPa as the diameter decreases from 250 to 150 nm. These values of the elastic modulus were significantly higher than the PVA bulk modulus of 1.7 GPa [35]. We anticipated the elastic modulus of PVA fibers would increase continually as the diameter decreases below 150 nm. Similar size-dependent effects were observed for other electrospun polymer fibers [36,37] which could be attributed to the size increase of the supramolecular structure [36], consisting of aligned domains of the polymer chains. These results showed that the diameter onset of this size-dependent effect was polymer dependent. Elastic moduli in the comparison study [36] were reported to increase exponentially over a wider diameter range than as our suggested data (Fig. 3c). The excess LSA integrated into the PVA was expected to minimize the size-dependent effect on PVA fibers as well as reduce the overall elastic modulus of the matrix. As shown in Fig. 3b, LSA significantly minimized the change in the elastic modulus with values ranging from 2.9 to 5.4 GPa for the diameter range of 142–255 nm. This measurement was necessary

to assess the effect of the change in the elastic moduli of PVA-LSA-CNT hybrid fibers (in the same diameter range) induced by CNT reinforcement. As a result, the data (Fig. 3a) from all studied PVA-LSA-CNT fibers illustrated a significantly higher degree of scattering in the elastic modulus, but no significant diameter dependency. However, we observed a significant 33% overall improvement of elastic modulus for the PVA-LSA-CNT system relative to the PVA-LSA matrix. This allowed us to experimentally investigate the CNT reinforcement effect introduced into the nanometer matrix based on the loading and aspect ratio of CNTs.

3.3. *Effect of the CNT loading on the elastic modulus*

The amount of CNTs in each PVA-LSA-CNT fiber was determined by analyzing high resolution-TEM micrographs using the Java-based image processing program ImageJ (National Institutes of Health, Bethesda, MD). Several TEM images were captured along the suspended section of the hybrid fibers on the TEM grid, and combined to provide one composite image in Fig. 4 (showing the same fiber as in Fig. 2). The average diameter of CNTs in the hybrid fibers is $d = 4.3$ nm with a standard deviation of 0.4 nm. The total CNT cross-sectional area was calculated by multiplying the sum of the contour length projected on the TEM image plane for every CNT in each hybrid fiber. The cross-sectional area of each hybrid fiber was calculated from the surface outline based on the composite TEM image. The percentage of the total CNT cross-sectional area in the hybrid fiber in Fig. 4 is 23 ± 2% (cross-sectional area fraction). For all studied hybrid fibers, the average CNT area fraction (±SE) was 16 ± 5% (a maximum of 26% and a minimum of 7%).

The data set was divided into 5 groups and plotted against the average elastic modulus (±SE) of each group in Fig. 5. The average elastic modulus of PVA-LSA fibers is shown as the first data point at the left. The last data point for 23–27% was based on one entry and thus excluded from further analysis. One-way ANOVA tests show that the elastic modulus of the hybrid fibers did not significantly vary between the 4 intervals of the CNT cross-sectional area fraction. No significant improvement in the elastic modulus over PVA-LSA fibers was observed regardless of the amount of CNTs.

Of interest was the comparison of the LSA dispersion method with other surfactant-based dispersion methods [38] such as sodium dodecyl sulfate for PVA-CNT hybrid fibers. Our procedure was able to fabricate hybrid fibers with consistently high CNT loading as indicated by Raman spectra (Fig. 1b) and TEM (Fig. 4). The CNT loading was measured from the composite TEM images with the results presented as the CNT cross-sectional area fraction. Within the average area of 200 nm (diameter) × 4.7 μm (length), the values varied from 7% to 26% for all studied hybrid fibers. This method generally undervalued the true loading inside the fiber because TEM could not identify overlapped CNTs along the electron beam. However, the distribution of the CNT loading in each hybrid fiber clearly demonstrated that imperfect dispersion and agglomeration significantly affected the uniformity of the CNT loading in a nanoscale matrix. Therefore, we anticipated heterogeneous properties in terms of CNT-induced functionalities at the nanoscale of hybrid fibers. For future studies, it is of utmost importance to determine the physical CNT loading in the fibers instead of using the nominal CNT loading in the solution in order to obtain proper results.

Fig. 4 – A composite picture of four TEM images taken from different part of the same hybrid fiber as shown in Fig. 2.

Fig. 5 shows no significant difference in elastic modulus among the six data intervals of the CNT loading. Such data were not in agreement with theoretical prediction [17], in which mechanical properties should increase as loading increases. These physical models, however, are based on several restrictive idealized assumptions for CNTs such as a fixed aspect ratio, uniform dispersion with no agglomeration and an aligned orientation in the composite materials. Our experimental data suggested that once CNT loading reached

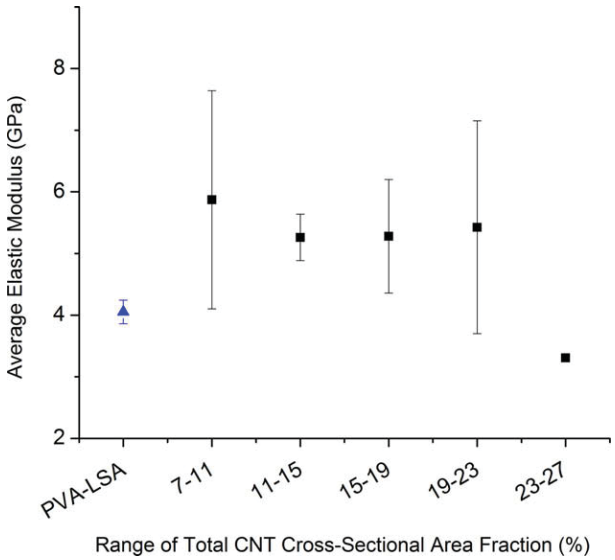

Fig. 5 – A profile of the average elastic modulus in each total CNT cross-sectional area fraction range of PVA-LSA-CNT fibers (square) and PVA-LSA fibers (triangle).

a certain level, the CNTs inevitably formed bundles or clusters and distributed non-uniformly as a segment of a hybrid fiber shown in Fig. 6. Accordingly, most physical simulations tend to overestimate the mechanical properties of the composite system at high levels of CNT loading [39], especially for systems with nanoscale morphologies. This was the main reason that an increase of area fraction from 7% to 26% in the CNT loading failed to steadily improve the stiffness of PVA-LSA-CNT fibers.

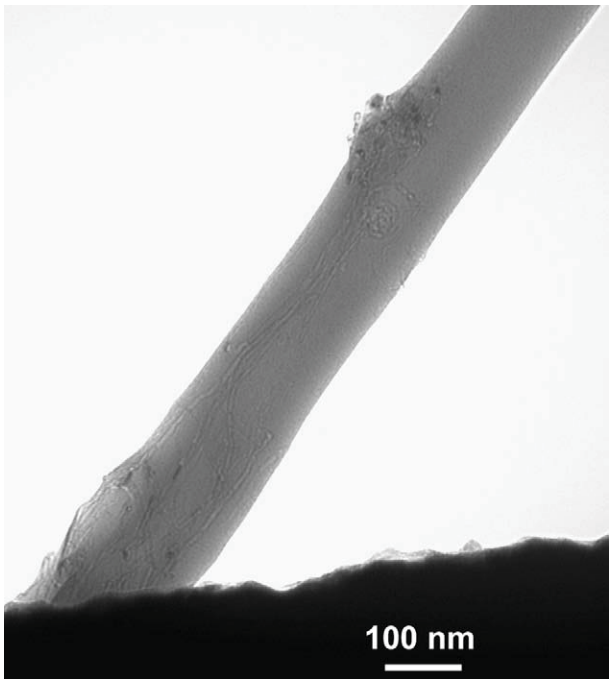

Fig. 6 – A TEM image of segment of a hybrid fiber with cluster of coiled/bundled CNTs.

3.4. *Effect of the CNT aspect ratio on the elastic modulus*

The displacement length of each CNT was also measured from the composite TEM images. Clusters with multiple CNT coiled together as shown in Fig. 6 were treated as one individual CNT. Data were then converted to a projected length (l) parallel to the axis of the hybrid fiber. With the average diameter (d) of CNTs introduced in the previous section, we determined the effective CNT aspect ratio (l/d) for each hybrid fiber.

Fig. 7 is a plot of the CNT aspect ratio distribution fitted with a lognormal distribution function for the hybrid fiber shown in Fig. 4. The standard deviation (σ) of this lognormal fit is 0.45 ± 0.06. For all studied hybrid fibers, the value of σ varied from 0.34 to 0.81, with an average value of 0.55 ± 0.13. The average CNT aspect ratio of the hybrid fiber was estimated to be 36, ranging from 13 to 83 as shown in Fig. 4. For all hybrid fibers, the average CNT aspect ratio (±SE) was 34 ± 5 (maximum = 43 and minimum = 24).

In Fig. 8, the average CNT aspect ratio of the hybrid fibers was divided into 5 groups and plotted against the average elastic modulus (±SE) of each group. The average elastic modulus of PVA-LSA fibers was included in the plot at the left. One-way ANOVA tests confirmed no significant difference in elastic modulus between PVA-LSA fibers and the first three groups of hybrid fibers. Starting from the group of 36–40, the average elastic modulus increased significantly ($P < 0.01$) compared to PVA-LSA fibers, but remained insignificantly different to the first three groups of hybrid fibers with the lower average aspect ratio ranges. The last group at 40–44 exhibited an average elastic modulus significantly different ($P < 0.01$) to all first four groups except for the group of 36–40.

To investigate the effect of CNT aspect ratio (l/d) on the elastic modulus of a hybrid fiber, the projected length (l) of CNTs was determined using the method described above. This was correlated to the basic physical assumptions for CNTs in the physical models [17]. For simplification, those studies always assume that CNT is straight and aligned in the matrix with no curling or buckling. The distribution of

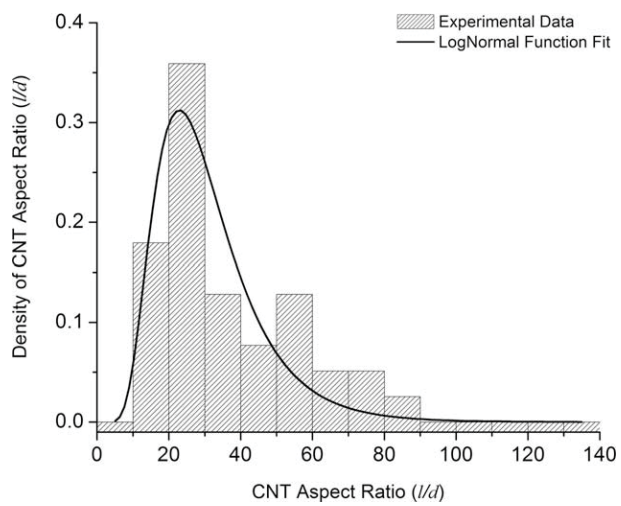

Fig. 7 – A plot of CNT aspect ratio distribution with lognormal distribution function fit.

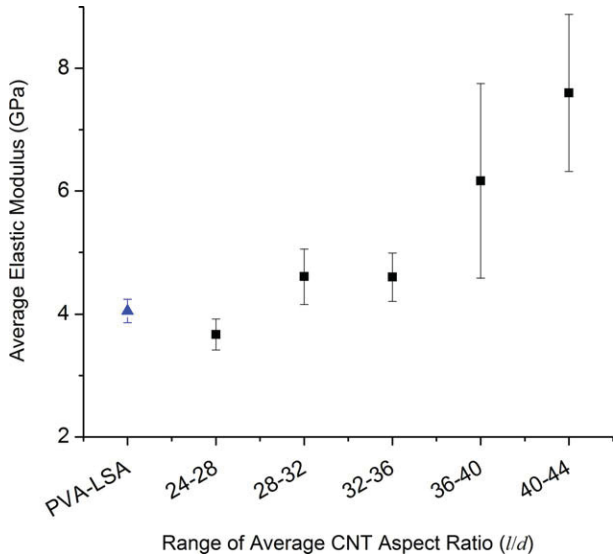

Fig. 8 – A profile of the average elastic modulus in each average CNT aspect ratio range of PVA-LSA-CNT fibers (square) and PVA-LSA fibers (triangle).

the CNT aspect ratio inside each fiber was expected to closely resemble the distribution in the solution, i.e. both dispersion and agglomeration were neglected. Our data show, however, that the distribution of the CNT aspect ratio (e.g. in Fig. 7) in all studied hybrid fibers was different. The average value of the CNT aspect ratio in the hybrid fibers varied from 24 to 43. However, the average value of the aspect ratio could not represent the state of stress transfer for all CNTs loaded in the matrix without considering the distribution of the aspect ratio. As Jiang et al. [40] concluded, the symmetry of the aspect ratio distribution can significantly affect the overall mechanical properties as a function of the CNT loading. We used a lognormal distribution function to fit the aspect ratio distribution. The standard deviation (σ) of the lognormal function (defining the symmetry of the distribution) was determined from the fit with a range of 0.34 to 0.81 for all studied hybrid fibers. Thus, the results were not sufficient to correlate the parameter σ to the elastic modulus of the hybrid fibers. However, Fig. 8 revealed that a significant improvement in the elastic modulus of the hybrid fibers was observed as the average value of the aspect ratio reached above 36. These values fall into the range (between 10 and 50) in which dramatic changes in the stress transfer along CNT has been predicted [21] in both an analytical model and a finite element model for the longitudinal modulus. This clearly indicated a significant role of the CNT aspect ratio in CNT reinforcement which affected the effectiveness of the stress transfer at any given CNT loading.

4. Conclusions

LSA was capable of dispersing CNTs in water and PVA for the preparation of hybrid fibers using the electrospinning technique. The elastic modulus of PVA-LSA-CNT hybrid fibers was comparable to that of PVA and PVA-LSA fibers. PVA fibers exhibited a size-dependence of the elastic modulus, i.e. the moduli increase with decreasing fiber diameter. With LSA added into the PVA matrix, the overall elastic modulus decreased by 71%. In turn, PVA-LSA-CNT fibers with an elastic modulus 33% higher than PVA-LSA fibers did not display a theoretically predicted improvement over PVA fibers. Such behavior suggested that another approach is needed to further improve the mechanical properties of the PVA system. Despite sonication and use of LSA, bundling and non-uniform dispersion of CNTs still occurs in each fiber. As a result, the CNT loading in all studied PVA-LSA-CNT fibers varied between 7% and 26%, different significantly from the nominal loading in the solution. The CNT loading shows no correlation to the elastic modulus. However, the increase of the average CNT aspect ratio from 24 to 43 was correlated with a significant upward trend in the elastic modulus of the hybrid fibers as predicted, regardless of the CNT loading and the fiber diameter. As the efficiency of the stress transfer in a composite matrix largely depends on the CNT aspect ratio, future improvement of mechanical properties should focus on maximizing the CNT reinforcement effect, based on the aspect ratio of CNTs rather than the CNT loading.

Acknowledgements

This work was supported by the Natural Sciences and Engineering Council of Canada (NSERC). We acknowledge technical assistance from Yali Liu (NRC), Keith Male (NRC).

REFERENCES

[1] Monthioux M, Kuznetsov VL. Who should be given the credit for the discovery of carbon nanotubes? Carbon 2006;44(9):1621–3.
[2] Radushkevich LV, Lukyanovich VM. Os ugleroda obrazujucegosja pri termiceskom razlozenii okisi ugleroda na zeleznom kontakte. Zurn Fisic Chim 1952;26:88–95.
[3] Cooper CA, Young RJ, Halsall M. Investigation into the deformation of carbon nanotubes and their composites through the use of Raman spectroscopy. Compos Part A: Appl Sci Manuf 2001;32(3–4):401–11.
[4] Kim YA, Muramatsu H, Hayashi T, Endo M, Terrones M, Dresselhaus MS. Thermal stability and structural changes of double-walled carbon nanotubes by heat treatment. Chem Phys Lett 2004;398(1–3):87–92.
[5] Tsai M-Y, Yu C-Y, Yang C-H, Tai N-H, Perng T-P, Tu Cn-M, et al. Electrical transport properties of individual disordered multiwalled carbon nanotubes. Appl Phys Lett 2006;89(19):192115-1–3.
[6] Brady-Estévez AS, Menachem ESK. A single-walled-carbon-nanotube filter for removal of viral and bacterial pathogens. Small 2008;4(4):481–4.
[7] Wang QH, Setlur AA, Lauerhaas JM, Dai JY, Seelig EW, Chang RPH. A nanotube-based field-emission flat panel display. Appl Phys Lett 1998;72(22):2912–3.
[8] Pumera M, Merkoçi A, Alegret S. Carbon nanotube-epoxy composites for electrochemical sensing. Sensor Actuator B: Chem 2006;113(2):617–22.
[9] Huang H, Liu CH, Wu Y, Fan S. Aligned carbon nanotube composite films for thermal management. Adv Mater 2005;17(13):1652–6.

[10] Foldvari M, Bagonluri M. Carbon nanotubes as functional excipients for nanomedicines: II Drug delivery and biocompatibility issues. Nanomedicine: Nanotechnol Biol Medicine 2008;4(3):183–200.
[11] Ajayan PM, Stephan O, Colliex C, Trauth D. Aligned carbon nanotube arrays formed by cutting a polymer resin-nanotube composite. Science 1994;265(5176):1212–4.
[12] Guhados G, Wan WK, Sun X, Hutter JL. Simultaneous measurement of Young's and shear moduli of multiwalled carbon nanotubes using atomic force microscopy. J Appl Phys 2007;101:033514-1–5.
[13] Coleman JN, Khan U, Blau WJ, Gun'ko YK. Small but strong: a review of the mechanical properties of carbon nanotube-polymer composites. Carbon 2006;44(9):1624–52.
[14] Kashiwagi T, Fagan J, Douglas JF, Yamamoto K, Heckert AN, Leigh SD, et al. Relationship between dispersion metric and properties of PMMA/SWNT nanocomposites. Polymer 2007;48(16):4855–66.
[15] Wang Q, Dai J, Li W, Wei Z, Jiang J. The effects of CNT alignment on electrical conductivity and mechanical properties of SWNT/epoxy nanocomposites. Compos Sci Technol 2008;68(7–8):1644–8.
[16] Gao J, Itkis ME, Yu A, Bekyarova E, Zhao B, Haddon RC. Continuous spinning of a single-walled carbon nanotube-nylon composite fiber. J Am Chem Soc 2005;127(11):3847–54.
[17] Tucker III CL, Liang E. Stiffness predictions for unidirectional short-fiber composites: review and evaluation. Compos Sci Technol 1999;59(5):655–71.
[18] Jeong JS, Moon JS, Jeon SY, Park JH, Alegaonkar PS, Yoo JB. Mechanical properties of electrospun PVA/MWNTs composite nanofibers. Thin Solid Film 2007;515(12):5136–41.
[19] Ayutsede J, Gandhi M, Sukigara S, Ye H, Hsu CM, Gogotsi Y, et al. Carbon nanotube reinforced bombyx mori silk nanofibers by the electrospinning process. Biomacromolecules 2006;7(1):208–14.
[20] Ryan KP, Cadek M, Nicolosi V, Blond D, Ruether M, Armstrong G, et al. Carbon nanotubes for reinforcement of plastics? A case study with poly(vinyl alcohol). Compos Sci Technol 2007;67(7–8):1640–9.
[21] Haque A, Ramasetty A. Theoretical study of stress transfer in carbon nanotube reinforced polymer matrix composites. Compos Struct 2005;71(1):68–77.
[22] Halpin Affdl JC, Kardos JL. The Halpin–Tsai equations: a review. Polym Eng Sci 1976;16(5):344–52.
[23] Badaire S, Poulin P, Maugey M, Zakri C. In situ measurements of nanotube dimensions in suspensions by depolarized dynamic light scattering. Langmuir 2004;20(24):10367–70.
[24] Dumitrica T, Hua M, Yakobson BI. Symmetry-, time-, and temperature-dependent strength of carbon nanotubes. 2006;103(16):6105–9.
[25] Jung S-W, Kim S-Y, Nam H-W, Han K-S. Measurements of fiber orientation and elastic-modulus analysis in short-fiber-reinforced composites. Compos Sci Technol 2001;61(1):107–16.
[26] Haggenmueller R, Zhou W, Fischer JE, Winey KI. Production and characterization of polymer nanocomposites with highly aligned single-walled carbon nanotubes. J Nanosci Nanotechnol 2003;3:105–10.
[27] Gao J, Yu A, Itkis ME, Bekyarova E, Zhao B, Niyogi S, et al. Large-scale fabrication of aligned single-walled carbon nanotube array and hierarchical single-walled carbon nanotube assembly. J Am Chem Soc 2004;126(51):16698–9.
[28] Liu Y, Gao L, Zheng S, Wang Y, Sun J, Kajiura H, et al. Debundling of single-walled carbon nanotubes by using natural polyelectrolytes. Nanotechnology 2007;18(36):365702-1–6.
[29] DeMerlis CC, Schoneker DR. Review of the oral toxicity of polyvinyl alcohol (PVA). Food Chem Toxicol 2003;41(3):319–26.
[30] Formhals A. US Patent 2187306 1940.
[31] Guhados G, Wan WK, Hutter JL. Measurement of the elastic modulus of single bacterial cellulose fiber using atomic force microscopy. Langmuir 2005;21(14):6642–6.
[32] Hutter JL, Bechhoefer J. Calibration of atomic-force microscope tips. Rev Sci Instrum 1993;64(7):1868–73.
[33] Abramova YI, Andreyev VI, Voskresenskii VA. Plasticizing effect of different types of aromatic compound on polyvinyl chloride (PVC). Polym Sci USSR 1967;9(11):2679–85.
[34] Kamoun A, Jelidi A, Chaabouni M. Evaluation of the performance of sulfonated esparto grass lignin as a plasticizer-water reducer for cement. Cement Concrete Res 2003;33(7):995–1003.
[35] Podsiadlo P, Kaushik Amit K, Arruda Ellen M, Waas Anthony M, Shim BS, Xu J, et al. Ultrastrong and stiff layered polymer nanocomposites. Science 2007;318(5847):80–3.
[36] Arinstein A, Burman M, Gendelman O, Zussman E. Effect of supramolecular structure on polymer nanofibre elasticity. Nature Nanotechnol 2007;2:59–62.
[37] Shin M-K, Kim Sun I, Kim S-J, Kim S-K, Lee H, Spinks GM. Size-dependent elastic modulus of single electroactive polymer nanofibers. Appl Phys Lett 2006;89:231929-1–3.
[38] Wang W, Ciselli P, Kuznetsov E, Peijs T, Barber AH. Effective reinforcement in carbon nanotube–polymer composites. Philos Trans Roy Soc A: Math Phys Eng Sci 2008;366(1870):1613–26.
[39] Eduljee RF, McCullough RL, Gillespie Jr JW. The influence of inclusion geometry on the elastic properties of discontinuous fiber composites. Polym Eng Sci 1994;34(4):352–60.
[40] Jiang B, Liu C, Zhang C, Wang B, Wang Z. The effect of non-symmetric distribution of fiber orientation and aspect ratio on elastic properties of composites. Compos Part B: Eng 2007;38(1):24–34.